Diagnosis of Pusher-Fuel Mix in Indirectly Driven Nova Implosions

T. R. Dittrich, B. A. Hammel, C. J. Keane, R. McEachern, R. E. Turner, S. W. Haan, and L. J. Suter
Lawrence Livermore National Laboratory, Livermore, California 94550
(Received 31 May 1994)

We report measurements of controlled implosion performance degradation arising from the Rayleigh-Taylor instability in inertial confinement fusion capsules. Using plastic capsules driven indirectly by the Nova laser, we studied the variation in implosion performance as a function of outer surface perturbation. Variations in both capsule x-ray and neutron emission are seen which are consistent with a model which describes mixing pusher material into fuel material. The model combines representative capsule surface characterization, implosion stability, and perturbation growth saturation.

PACS numbers: 52.25.Nr, 52.25.Tx, 52.50.Lp, 52.55.Pi

A key issue for inertial confinement fusion (ICF) is the hydrodynamic stability of the imploding capsule. Imperfections on the capsule surface can grow into large perturbations degrading capsule performance. Understanding this process is crucial if we are to successfully predict requirements for future high-gain ICF capsules. Experiments on the Nova laser have directly measured perturbation growth on planar foils [1], and three experimental groups have investigated backlit perturbation growth using imploding spheres [2–4]. In addition to these efforts which concentrate on indirectly driven implosions is work investigating the hydrodynamic stability of directly driven ICF capsules [5,6]. In these direct drive experiments the laser light directly shines on the capsules both causing the implosion and providing the seed for perturbation growth. This article reports measurement, via emission from spectroscopic tracers [7], of the full process of perturbation growth leading to pusher-fuel mix in spherical implosions and shows dependence on initial perturbation amplitude and wavelength. In contrast to the cited direct drive work we have here separated the drive from the perturbation seed. (For a review of x-ray spectroscopy of ICF plasmas see [8,9].)

The purpose of the experiments described here was to study, in a controlled manner, the effects of the Rayleigh-Taylor (RT) instability on capsule implosion performance. The mechanism by which RT growth degrades capsule performance can be summarized as follows. As the ablation phase of the implosion proceeds, surface imperfections grow via the RT instability as low density ablated material pushes on the high-density shell. This growth causes the imploding shock to deviate from spherical, carrying the perturbation information through the shell and rippling the interface between pusher and fuel. Later in time when the fuel is compressed, the pusher/fuel interface becomes RT unstable which causes this rippling to grow and produce a region of mixed pusher and fuel material. Increasing the initial outer surface perturbation increases the degree of pusher-fuel mixing.

These Nova experiments use deuterium-filled plastic-shelled capsules. A typical capsule shell had a 420 μm inside diameter, 55 μm thick wall, and consisted of three layers. The inner layer, the pusher, was $\approx$3 μm of polystyrene doped with 1.0% (atomic) chlorine. The middle layer was a 3 μm thick permeation barrier made of polyvinylalcohol (PVA) which sealed in the fuel gas. An outer layer of plasma polymer ($CH_{1.3}$) [10] was deposited over the inner layers, forming the ablator. The capsules were filled with 50 atm of deuterium gas and 0.1 atm argon.

These capsules were imploded by means of the Nova laser. A 1 ns duration, square pulse of laser light was converted to x rays which ablated the plastic and caused the implosion. This "indirect drive" was produced in a cylindrical gold case, or *Hohlraum,* was heated by typically 17 kJ of laser energy, and reached a peak radiation temperature of 230 eV. Capsules had relatively low convergence ($\approx$8) and had considerably less sensitivity to growth of surface perturbations compared to that predicted for current high-gain ICF capsule designs. This low convergence was intentionally chosen so that asymmetries in the x-ray drive would have little effect on the implosions and would, therefore, not complicate the perturbation growth effects.

To make capsules with various degrees of surface roughness, many polystyrene beads, ranging in diameter from 0.6 to 7 μm were embedded in the PVA layer. When the ablator layer was deposited onto this rough PVA surface, the perturbations were imprinted on the outer surface. This method of using a capsule with a controllably rough outer surface as seed for RT growth during implosion contrasts with the method used in [5,6] where direct drive laser illumination nonuniformity was assumed both to be the dominant source of initial amplitude seeds to the RT instability and to be representable by a semiempirical analytic expression.

After these capsules were shot we developed the capability of characterizing shell surfaces using an equatorially-tracing atomic force microscope (AFM). Using this AFM, traces were taken of capsules from the same production runs as those that were shot. (To verify surface similarity, scanning electron microscope images of these traced capsules were compared with images of the shot capsules.) The equatorial traces were converted to power spectra and combined to form

 0031-9007/94/73(17)/2324(4)$06.00

ensemble averages. By assuming that the surface bumpiness is isotropic, these one-dimensional average power spectra were transformed into two-dimensional (spherical surface) power spectra [11]:

$$P_{2D}(\ell) = \left(\ell + \frac{1}{2}\right) \sum_{n=\ell,\ell+2}^{\infty} [P_{1D}(n) - P_{1D}(n+2)] \times \frac{(n+\ell)!!(n-\ell-1)!!}{(n-\ell)!!(n+\ell+1)!!},$$

where ℓ is the perturbation mode number, P_{1D} is the one-dimensional power spectrum, and P_{2D} is the two-dimensional power spectrum. Figure 1 shows 2D (spherical surface) power spectra of capsules with rms = 0.03, 0.31, and 1.75 μm.

Diagnosis of enhanced pusher-fuel mix due to these surface perturbations was performed in two ways. First, the variation in capsule DD neutron yield with roughness was monitored; this is expected to decrease with increasing surface roughness as cold dense pusher material increasingly poisons the fuel. Second, the variation in the x-ray self-emission of included trace elements, or dopants [7,12], with roughness was monitored. The x-ray emission of the pusher dopant, chlorine, is expected to increase relative to the x-ray emission of the fuel dopant, argon, as the surface roughness is increased. In the present temperature and density regime the variation of x-ray line radiation from these dopants is strongly dependent on temperature. During the implosion, PdV work heats the fuel and the argon, but the chlorine is heated via conduction and convection due to mixing. At peak x-ray emission the imploded capsule has steep gradients through the mix region in both electron temperature and density as a function of radius. This makes a simple one-temperature, one-density understanding of this process difficult. Because of this, the x-ray emission was observed by means of a crystal spectrometer coupled to an x-ray streak camera. It has temporal resolution of $\approx$30 ps and a spectral resolving power ($\lambda/\delta\lambda$) of $\approx$700 [13].

Simulating the implosion of these capsules was a multistep process. First, we estimated the capsule's sensitivity to surface perturbations using several 2D LASNEX [14] simulations, each of which estimated linear growth for a given single mode. The initial perturbations in these simulations were small to ensure that only linear growth would occur. This perturbation growth included the effects of stabilization at the ablation surface, feed-through between the interfaces, and Rayleigh-Taylor–Richtmyer-Meshkov instability growth at the pusher/fuel interface. Figure 2 plots these linear growth factors at the pusher/fuel interface versus perturbation mode number. This growth factor is the amplification of a perturbation initially on the outer surface as it imprints on the inner capsule surface. It is typically quoted at peak neutron emission. Negative growth factor values indicate phase change of the perturbation. This linear perturbation growth is small relative to high-gain ICF capsules because of favorable stabilization mechanisms at the ablation surface.

Next, we combined the surface roughness, $P_{2D}(\ell)$, with the linear perturbation growth factors per standard linear analysis. Nonlinear saturation was estimated with Haan's criterion [15] which states that saturation occurs on a spherical surface of radius R when amplitudes become larger than $4R/\ell^2$. These saturated amplitudes then grow at a constant rate, rather than exponentially. This procedure predicted the pusher-fuel mixing versus time, estimated from the calculated rms deviation, σ, of the pusher-fuel surface from spherical. The limit of the bubble tips outward is taken to be $\sqrt{2}\sigma$, and the extent of spike tips inward to be $(1 + A)\sqrt{2}\sigma$, where A is the Atwood number. Also included in this mix region size estimate were contributions from both initial pusher-fuel surface imperfections and effects of embedding microspheres in the PVA layer of some of the capsules

Atomic mixing of the pusher and fuel is assumed throughout the mixed region. This modeling distributes the materials within this region so as to maintain a constant concentration while conserving individual material amounts.

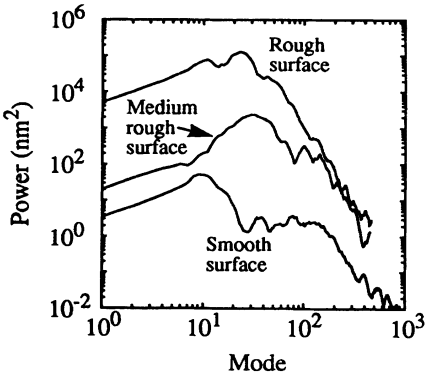

FIG. 1. The 2D (spherical surface) power spectra characterizing the outer surface of three representative capsules with rms = 0.03, 0.31, and 1.70 μm.

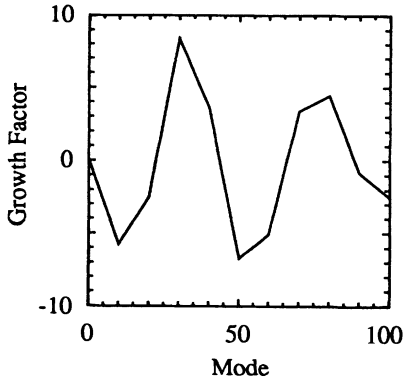

FIG. 2. Growth factor at pusher/fuel interface vs mode number for perturbations initially on the capsule outer surface. This is a snapshot at time of peak neutron production. Negative values indicate phase change of the perturbation.

TABLE I. Nova shots in the Ar/Cl implosion series.

Shot	Imbedded bead diameter (μm)	Surface rms (μm)	Observed yield (10^9 neut.)	Observed yield/ Clean (no mix) yield
1	none	0.031	1.21	0.72
2	none	0.031	1.26	0.83
3	none	0.064	0.53	0.33
4	none	0.065	1.01	0.60
5	0.6	0.307	0.60	0.35
6	2.0	0.308	1.22	0.49
7	2.0	0.308	0.65	0.44
8	3.9–7.0	1.70	0.66	0.20
9	3.9–7.0	1.70	0.70	0.20

Finally, implosion simulations via LASNEX used this time-dependent mix region in a self-consistent manner (i.e., the mixing affected the hydrodynamic evolution) and generated emission spectra by means of detailed configuration accounting (DCA) [16,17]. These 1D simulations used detailed atomic models for both argon and chlorine. The DCA simulated spectra were calculated using 69 and 70 level models for chlorine and argon, respectively. The models were produced by the DSP [18] code which contains atomic physics identical to that used in the RATION code [19].

Table I lists the nine Nova shots which comprise this experimental series along with capsule surface conditions and observed and simulated yields. We have chosen three of these shots to illustrate the variation in x-ray spectral output during implosion with initial capsule surface roughness.

Figure 3 shows spectra at peak x-ray emission for the implosion of a smooth (0.03 μm rms) capsule. Figure 3(a) shows the spectrum observed with the spectrometer, and Fig. 3(b) shows the analogous DCA simulated spectrum. Very little chlorine Ly-α emission, relative to argon Ly-α, is evident in either of these spectra. The simulations indicate that 6% of the total chlorine mass has reached at least 600 eV. The simulated Ly-α satellite line

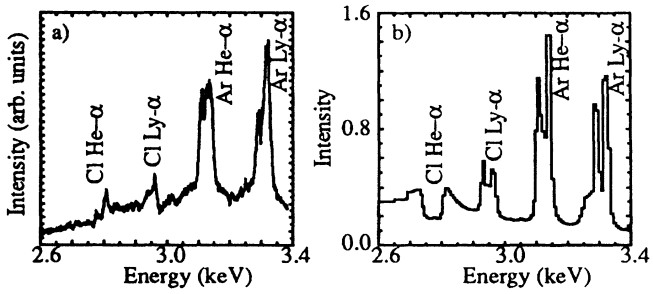

FIG. 3. Spectra at peak x-ray emission from the implosion of a smooth surface (rms = 0.03 μm) capsule. (a) is as observed by the streaked crystal spectrometer. (b) is the 1D DCA simulation of this shot. Relevant emission lines of chlorine and argon are labeled. Intensity units are 10^{10} joules/sec/ster/keV.

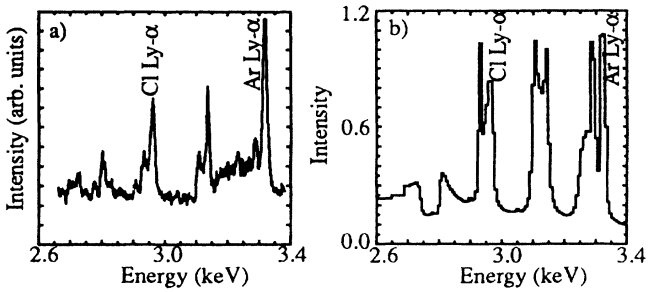

FIG. 4. Same as Fig. 3, for an intermediate roughness (rms = 0.3 μm) capsule.

strengths, on the low energy side of the Ly-α lines, differ from those observed and the large absorption feature evident in Fig. 3(b) at 2.75–2.80 keV is probably due to errors in calculating the opacity of the chlorine He-α line in the colder plastic away from the pusher/fuel interface. Figure 4 shows the spectra from an intermediate roughness (0.31 μm rms) capsule. In this case the Ly-α emission from both the chlorine and argon are comparable in strength, and 10% of the total chlorine mass (according to simulation) has reached at least 600 eV. Figure 5 shows the spectra from a very rough (1.75 μm rms) capsule. In this case the chlorine Ly-α emission is stronger than the argon Ly-α emission and 15% of the total chlorine mass (according to simulation) has reached at least 600 eV. The simulations show that from smooth to rough surface capsules the chlorine Ly-α emission increased by 350% while the argon Ly-α emission decreased by 30%.

To quantitatively compare the observed and simulated spectra we ratio the time-integrated Ly-α emission from the two dopants. (At each time this line emission was estimated by subtracting the continuum and background and deconvolving the result into distinct Gaussian-shaped peaks. In this manner contributions from the strong satellite lines of the Ly-α transitions and the chlorine He-β line at 3.27 keV were eliminated.) The argon Ly-α strength effectively normalizes the chlorine Ly-α strength to the specifics of capsule performance such as capsule size, laser drive, and diagnostic calibration.

This comparison of observed and simulated emission spectra by means of the ratio of time-integrated Ly-α

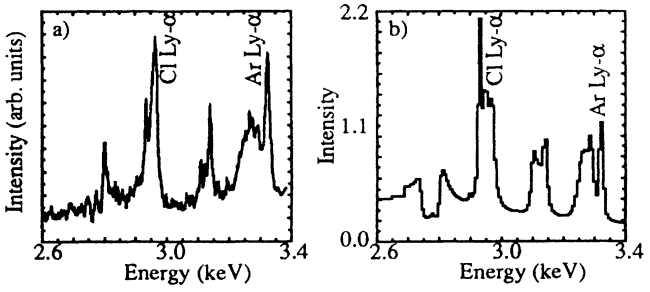

FIG. 5. Same as Fig. 3, for a very rough (rms = 1.7 μm) capsule.

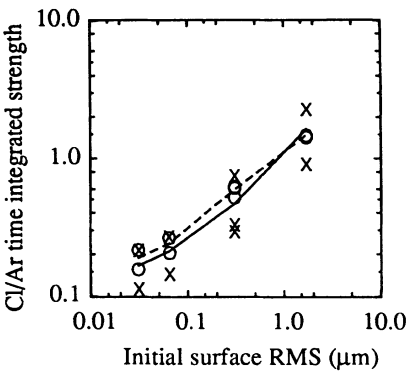

FIG. 6. Comparison of simulated and observed emission spectra from the nine shots in the series. The ratio of time-integrated chlorine and argon Ly-α emission is plotted vs surface finish. X marks experimental points; O marks simulation points. The solid line and dashed lines are the results of averaging the experimental and simulation values, respectively, at each distinct rms value.

lines is shown in Fig. 6 for all nine shots. The ratio of emission strength smoothly changed a factor of ≈ 9 for a surface rms change of ≈ 50. Figure 7 shows observed and simulated mixed neutron yield over clean yield versus rms surface finish for the same nine-shot data set.

To test the importance of the saturation modeling, we also estimated the perturbation growth with unmodified linear analysis. The modification due to saturation is quite small, and, given the large spread in experimental results, no conclusion can be made regarding the correctness of the saturation modeling procedure.

In conclusion, both the observed x-ray emission and neutron yield from the 1 ns drive Nova implosions show significant variation as a function of initial capsule surface finish. Furthermore, this variation can be successfully interpreted as a dependence of pusher-fuel mixing on initial surface roughness. This interpretation consists of modeling based on linear analysis using multiple 2D LASNEX simulations and 1D mixed implosion modeling using LASNEX and DCA to simulate neutron output and x-ray emission of included dopants.

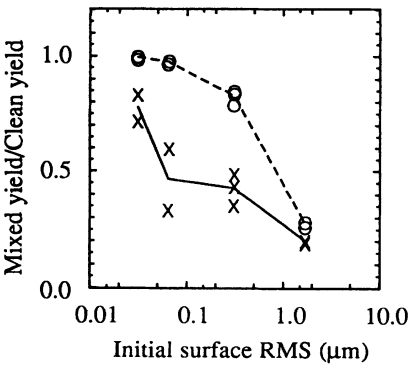

FIG. 7. Observed and simulated mixed neutron yield over clean yield vs surface finish for the same nine-shot data set. Legend per Fig. 6

The authors wish to thank Craig Moore for his efforts in capsule characterization, Ravi Upadhye and Blanca Haendler for their early work in rough-surfaced capsule fabrication, and Steve Langer, Steve Hatchett, and Yim Lee for assistance in simulation details. This work was performed under the auspices of the U.S. Department of Energy by the Lawrence Livermore National Laboratory under Contract No. W-7405-ENG-48.

[1] B. A. Remington, S. V. Weber, S. W. Haan, J. D. Kilkenny, S. G. Glendinning, R. J. Wallace, W. H. Goldstein, B. G. Wilson, and J. K. Nash, Phys. Fluids B **5**, 2589–2595 (1993).
[2] J. S. Wark, J. D. Kilkenny, A. J. Cole, M. H. Key, and P. T. Rumsby, Appl. Phys. Lett. **48**, 969–971 (1986).
[3] H. Nishimura, H. Takabe, K. Mima, F. Hattori, H. Hasegawa, H. Azechi, M. Nakai, K. Kondo, T. Norimatsu, Y. Izawa, C. Yamanaka, and S. Nakai, Phys. Fluids **31**, 2875–2883 (1988).
[4] W. Mead and A. Hauer (private communication).
[5] D. K. Bradley, J. A. Delettrez, and C. P. Verdon, Phys. Rev. Lett. **68**, 2774–2777 (1992).
[6] J. Delettrez, D. K. Bradley, P. A. Jaanimagi, and C. P. Verdon, Phys. Rev. A **41**, 5583–5593 (1990).
[7] B. A. Hammel, C. J. Keane, T. R. Dittrich, D. R. Kania, J. D. Kilkenny, R. W. Lee, and W. K. Levedahl, J. Quant. Spectrosc. Radiat. Transfer **51**, 113–124 (1994).
[8] A. A. Hauer, N. D. Delamater, and Z. M. Koenig, Laser and Particle Beams **9**, 3–48 (1991).
[9] C. J. Keane, B. A. Hammel, D. R. Kania, J. D. Kilkenny, R. W. Lee, A. L. Osterheld, L. J. Suter, R. C. Mancini, C. F. Hooper, Jr., and N. D. Delamater, Phys. Fluids B **5**, 3328–3336 (1993).
[10] S. A. Letts, D. W. Meyers, and L. A. Witt, J. Vac. Sci. Technol. **19**, 739–742 (1981).
[11] S. Pollaine (private communication).
[12] B. A. Hammel, C. J. Keane, M. D. Cable, D. R. Kania, J. D. Kilkenny, R. W. Lee, and R. Pasha, Phys. Rev. Lett. **70**, 1263–1266 (1993).
[13] B. A. Hammel, P. Bell, C. J. Keane, R. W. Lee, and C. L. S. Lewis, Rev. Sci. Instrum. **61**, 2774–2776 (1990).
[14] G. B. Zimmerman and W. L. Kruer, Comments Plasma Physics Controlled Fusion **2**, 51–61 (1975).
[15] S. W. Haan, Phys. Rev. A **39**, 5812 (1989).
[16] Y. T. Lee, D. S. Bailey, and G. B. Zimmerman, in Laser Program Annual Report 1985, LLNL Report No. UCRL-50021-85, 1985, pp. 2.81–2.86.
[17] Y. T. Lee, J. Quant. Spectrosc. Radiat. Transfer **38**, 131–145 (1987).
[18] C. J. Keane, R. W. Lee, and J. P. Grandy, in *Proceedings of the 4th International Workshop on the Radiative Properties of Hot Dense Matter,* edited by W. Goldstein, C. Hooper, J. Gauthier, J. Seely, and R. W. Lee (World Scientific, Singapore, 1991), p. 233.
[19] R. W. Lee, B. L. Whitten, and J. E. Strout III, J. Quant. Spectrosc. Radiat. Transfer **32**, 91 (1984).